Dicopper(II) Complexes Bridged by Single N−N Bonds. Magnetic Exchange Dependence on the Rotation Angle between the Magnetic Planes

Zhiqiang Xu, Laurence K. Thompson,* and David O. Miller

Department of Chemistry, Memorial University of Newfoundland, St. John's, Newfoundland A1B 3X7, Canada

Received February 27, 1997[⊗]

A series of dicopper(II) complexes with two tetradentate (N_4) diazine ligands (PAHAP (**1**), PMHAP (**2**)) is reported, in which the two $d_{x^2-z^2}$ type copper centers are bridged by a single N−N bond. Varying the coligands leads to a situation where the angle between the copper planes can be varied. For small angles (<80°) ferromagnetic coupling prevails, whereas at larger angles antiferromagnetic exchange is observed between the copper(II) centers. This is associated with the degree of alignment of the nitrogen p orbitals in the diazine bridge, and is supported by molecular orbital calculations on the complexes and appropriate models. Structures are reported for PAHAP (**1**) (picolinamide azine), $[Cu_2(PAHAP)Cl_4]\cdot H_2O$ (**3**), $[Cu_2(PAHAP)Br_4]\cdot H_2O$ (**5**), $[Cu_2(PAHAP)(H_2O)_6](NO_3)_4$ (**6**), and $[Cu_2(PMHAP\text{-}H)(NO_3)_3]$ (**8**). **1** crystallized in the orthorhombic system, space group *Pbca* (No. 61), with $a = 19.845(4)$ Å, $b = 13.178(5)$ Å, $c = 9.383(8)$ Å, and $Z = 8$. **3** crystallized in the monoclinic system, space group *C*2/*c* (No. 15), with $a = 26.732(6)$ Å, $b = 8.670(9)$ Å, $c = 16.436(4)$ Å, $\beta = 100.88(2)°$, and $Z = 8$. **5** crystallized in the monoclinic system, space group *C*2/*c* (No. 15), with $a = 27.336(2)$ Å, $b = 8.859(4)$ Å, $c = 16.795(3)$ Å, $\beta = 100.78(1)°$, and $Z = 8$. **6** crystallized in the monoclinic system, space group *C*2/*c* (No. 15), with $a = 20.983(4)$ Å, $b = 7.505(4)$ Å, $c = 17.219(3)$ Å, $\beta = 104.22(1)°$, and $Z = 4$. **8** crystallized in the triclinic system, space group $P\bar{1}$ (No. 2), with $a = 7.8380(14)$ Å, $b = 8.015(3)$ Å, $c = 15.655(4)$ Å, $\alpha = 99.81(3)°$, $\beta = 101.74(2)°$, $\gamma = 94.524(17)°$, and $Z = 2$. The antiferromagnetically coupled complexes $[Cu_2(PAHAP)Cl_4]$ (**4**) and $[Cu_2(PAHAP\text{-}H)(N_3)_2(NO_3)]$ (**7**) are also reported.

Introduction

N_2 diazine bridges in, for example, polyfunctional pyrazole, triazole, pyridazine and phthalazine ligands bring two copper(II) centers into close proximity and provide an intramolecular exchange pathway for spin exchange interactions.[1−15] Exchange integrals ($-2J$) vary depending on the nature of the heterocyclic ring and the extent of double-bond character in the N−N bond. For essentially planar bis(N_4 ligand) complexes (Figure 1; **I**−**VII**) involving $d_{x^2-y^2}$ ground state copper(II) centers $-2J$ values follow the order pyridazine/phthalazine[9,12,16] (450−550 cm^{-1}) > pyrazolate[1−3] (200−430 cm^{-1}) > triazolate[4,7] (200−240 cm^{-1}) > 4-aminotriazole[5,16] (<220 cm^{-1}). Generally antiferromagnetic coupling increases as N−N distance decreases. Whether this is associated with increased π interactions or simply a shorter bridge distance and greater σ overlap is not clear, but in the case of the aminotriazole ligands, π-conjugation within the heterocyclic ring is likely to be weak or nonexistent. Although no examples of planar 2:2 dicopper(II) complexes of thiadiazole ligands (Figure 1; **VIII**) are known, for 1:2 complexes relatively weak antiferromagnetic coupling is observed ($-2J < 70$ cm^{-1}),[17] despite quite short N−N distances (<1.36 Å), which are comparable with those found for the pyrazole bridged systems.

For these heterocyclic bis-diazine complexes (Figure 1; **I**−**VII**), the adjacent pairs of nitrogen atoms are effectively locked into a conformation that allows only limited twisting of the copper planes by rotation about the copper-nitrogen bonds. In this situation, there would be optimal overlap between the copper magnetic orbitals and appropriate orbitals on the diazine nitrogen atoms. In the complex $[Cu_2(PTP)_2Cl](ClO_4)_3$ (PTP = 3,6-bis(2-pyridylthio)pyridazine; Figure 1; **IX**), the copper N_4 coordination planes are canted symmetrically toward an apical chlorine bridge in a boat conformation.[18] Surprisingly, this situation does not appear to diminish antiferromagnetic exchange significantly ($-2J = 479(1)$ cm^{-1}), with an exchange integral comparable to that observed for the planar complex [Cu_2-

* Corresponding author.

⊗ Abstract published in *Advance ACS Abstracts,* August 1, 1997.

(1) Kamiusuki, T.; Ōkawa, H.; Matsumoto, N.; Kida, S. *J. Chem. Soc., Dalton Trans.* **1990**, 195.
(2) Bayon, J. C.; Esteban, P.; Net, G.; Rasmussen, P. G.; Baker, K. N.; Hahn, C. W.; Gumz, M. M. *Inorg. Chem.* **1991**, *30*, 2572.
(3) Pons, J.; López, X.; Casabó, J.; Teixidor, F.; Caubet, A.; Ruis, J.; Miravitlles, C. *Inorg. Chim. Acta* **1992**, *195*, 61.
(4) Bencini, A.; Gatteschi, D.; Zanchini, C.; Haasnoot, J. G.; Prins, R.; Reedijk, J. *Inorg. Chem.* **1985**, *24*, 2812.
(5) Koomen-van Oudenniel, W. M. E.; de Graff, R. A. G.; Haasnoot, J. G.; Prins, R.; Reedijk, J. *Inorg. Chem.* **1989**, *28*, 1128.
(6) van Koningsbruggen, P. J.; Gatteschi, D.; de Graff, R. A. G.; Haasnoot, J. G.; Reedijk, J.; Zanchini, C. *Inorg. Chem.* **1995**, *34*, 5175.
(7) Prins, R.; Birker, P. J. M. W. L.; Haasnoot, J. G.; Verschoor, G. C.; Reedijk, J. *Inorg. Chem.* **1985**, *24*, 4128.
(8) Slangen, P. M.; van Koningsbruggen, P. J.; Haasnoot, J. G.; Jansen, J.; Gorter, S.; Reedijk, J.; Kooijman, H.; Smeets, W. J. J.; Spek, A. L. *Inorg. Chim. Acta* **1993**, *212*, 289.
(9) Abraham, F.; Lagrenee, M.; Sueur, S.; Mernari, B.; Bremard, C. *J. Chem. Soc., Dalton Trans.* **1991**, 1443.
(10) Mandal, S. K.; Thompson, L. K.; Newlands, M. J.; Lee, F. L; LePage, Y.; Charland, J.-P.; Gabe, E. J. *Inorg. Chim. Acta* **1986**, *122*, 199.
(11) Thompson, L. K.; Mandal, S. K.; Charland, J.-P.; Gabe, E. J. *Can. J. Chem.* **1988**, *66*, 348.
(12) Tandon, S. S.; Thompson, L. K.; Hynes, R. C. *Inorg. Chem.* **1992**, *31*, 2210.
(13) Chen, L.; Thompson, L. K.; Bridson, J. N. *Inorg. Chem.* **1993**, *32*, 2938.
(14) Thompson, L. K.; Tandon, S. S.; Manuel, M. E. *Inorg. Chem.* **1995**, *34*, 2356.
(15) Tandon, S. S.; Thompson, L. K.; Manuel, M. E.; Bridson, J. N. *Inorg. Chem.* **1994**, *33*, 5555.
(16) van Koningsbruggen, P. J.; Haasnoot, J. G.; de Graff, R. A. G.; Reedijk, J.; Slingerland, S. *Acta Crystallogr.* **1992**, *C48*, 1923.
(17) Tandon, S. S.; Chen, L.; Thompson, L. K.; Bridson, J. N. *Inorg. Chem.* **1994**, *33*, 490.
(18) Mandal, S. K.; Thompson, L. K.; Gabe, E. J.; Charland, J.-P.; Lee, F. L. *Inorg. Chem.* **1988**, *27*, 855.

S0020-1669(97)00235-8 CCC: $14.00

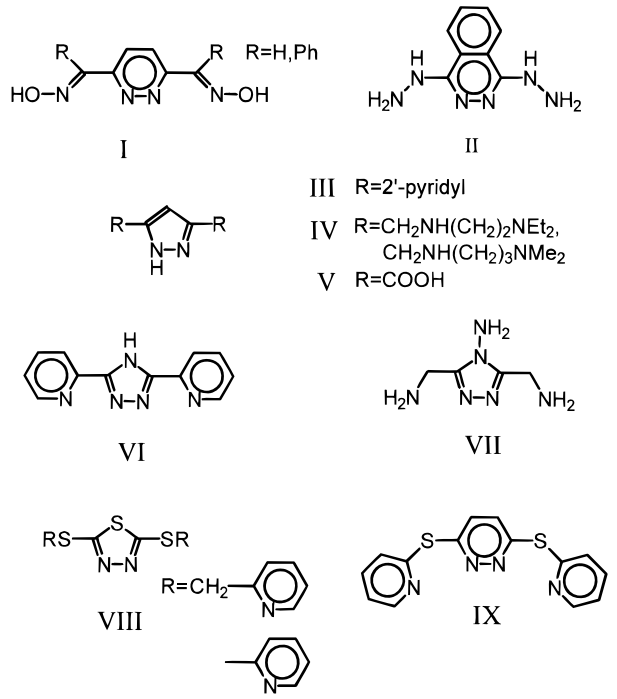

Figure 1. Dinucleating diazine ligands.

$(DHPH)_2(H_2O)_2](ClO_4)_4$ (Figure 1; **II** = DHPH).[12] This observation agrees with a theoretical study on a square planar bis(μ-pyrazolato)dicopper(II) model complex, $[Cu_2(pyz)_2Cl_4]^{2-}$, which showed that the energy difference between the two highest occupied molecular orbitals in the triplet state was insensitive to the twisting of the copper planes relative to the pyrazolate planes, and vice versa.[19a] However this contrasts with Kahn's theoretical study on *roof-shaped* bis(hydroxo)-bridged dicopper(II) model complexes, which shows that J_{AF} diminishes as the dihedral angle between the copper planes decreases.[19b]

The ligands PAHAP (picolinamide azine)[20] and PMHAP (Figure 2), which are derived from hydrazine, present an unusual arrangement of potential donor sites, with many possible mononucleating and dinucleating coordination modes. Two possible *trans*-dinucleating modes for PAHAP (Figure 2a,b) involve simultaneous coordination of pyridine and diazine nitrogens, in one case, and pyridine and amino nitrogens, in the other. Free rotation about the N−N single bond would lead to both folded *trans* and *cis* conformations. PAHAP has the potential for hexadentate coordination in a dinuclear complex (Figure 2c), while for PMHAP the limit would be pentadentate. PAHAP resembles the ligands PMK (bis(2-pyridylmethyl)-ketazine)[21] and PAA (2-pyridinecarbaldazine).[22−24] To our knowledge, there is only one structurally documented dicopper-(II) complex of these ligands, $[Cu_2(PMK)Cl_4]$,[21] which has a folded square-planar *cis* conformation (Figure 2a), with an acute angle between the copper planes (Cu−N−N−Cu torsion angle 70.8°). This complex exhibits weak antiferromagnetic coupling ($-2J$ = 52 cm^{-1}). A related complex with a fixed *trans* conformation, $[Cu_2(HL')Cl_3(H_2O)]\cdot 1.5H_2O$[25] ($H_2L'$ = bis(methyl 2-pyridyl ketone) carbonohydrazone), and an almost planar

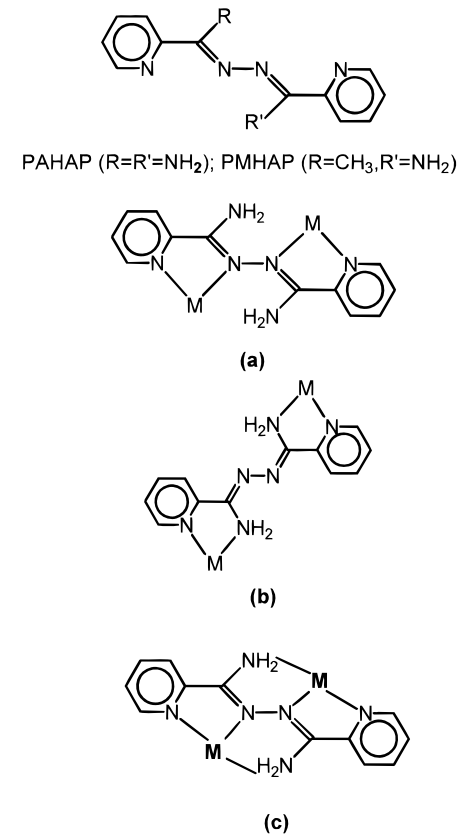

Figure 2. Picolinamide azines (PAHAP, PMHAP) and their coordination modes.

arrangement of two $d_{x^2-y^2}$ copper(II) centers with respect to the N−N bond exhibits strong antiferromagnetic coupling ($-2J$ = 213.3 cm^{-1}). A few other reports document the structures of dinuclear copper(II) complexes of hydrazone ligands with nominally single N−N bridges, but no variable-temperature magnetic data have been reported.[26−29] The cyclic tetranuclear copper(II) complex of the asymmetric hydrazone ligand *N*-(iminopicolinyl)-*N*′-oxamylhydrazine (L) $\{[Cu(L\text{-}H)]_4(NO_3)_4(H_2O)_8\}$[30] has a 90° twist between the copper square planes bound to each half of the ligand around the N−N bond, resulting in a negligible exchange interaction between the metal centers.

In this report, structures are presented for the ligand PAHAP (**1**) and three of its complexes, $[Cu_2(PAHAP)Cl_4]\cdot H_2O$ (**3**), $[Cu_2(PAHAP)Br_4]\cdot H_2O$ (**5**), and $[Cu_2(PAHAP)(H_2O)_6](NO_3)_4$ (**6**), as well as the structure of $[Cu_2(PMHAP\text{-}H)(NO_3)_3]$ (**8**). Variable-temperature magnetic measurements reveal ferromagnetic behavior for **3** and **5** and antiferromagnetic behavior for **6** and **8**, which will be discussed in the light of twisting of the copper magnetic planes about the single N−N bond. These observations are supported by molecular orbital calculations at the extended Hückel level for the complexes themselves and also for realistic models. The complexes $[Cu_2(PAHAP)Cl_4]$ (**4**) and $[Cu_2(PAHAP\text{-}H)(N_3)_2(NO_3)]$ (**7**), which both exhibit antiferromagnetic coupling, are also reported but are not characterized structurally.

(19) (a) Ajò, D.; Bencini, A.; Mani, F. *Inorg. Chem.* **1988**, *27*, 2437. (b) Charlot, M. F.; Jeannin, S.; Jeannin, Y.; Kahn, O.; Lucrece-Abaul, J.; Martin-Frere, J. *Inorg. Chem.* **1979**, *18*, 1675.
(20) Case, F. H. *J. Heterocycl. Chem.* **1970**, *7*, 1001.
(21) O'Connor, C. J.; Romananch, R. J.; Robertson, D. M.; Eduok, E. E; Fronczek, F. R. *Inorg. Chem.* **1983**, *22*, 449.
(22) Stratton, W. J.; Busch, D. H. *J. Am. Chem. Soc.* **1958**, *80*, 1286.
(23) Stratton, W. J.; Busch, D. H. *J. Am. Chem. Soc.* **1960**, *82*, 4834.
(24) Ball, P. W.; Blake, A. B. *J. Chem. Soc. A* **1969**, 1415.
(25) Bacchi, A.; Bonini, A.; Carcelli, M.; Ferraro, F.; Leporati, E.; Pelizzi, C.; Pelizzi, G. *J. Chem. Soc., Dalton Trans.* **1996**, 2699.
(26) Koziol, A. E.; Palenik, R. C.; Palenik, G. J. *J. Chem. Soc., Chem. Commun.* **1989**, 650.
(27) Bachi, A.; Battaglia, L. P.; Carcelli, M.; Pelizzi, C.; Pelizzi, G.; Solinas, C.; Zoroddu, M. A. *J. Chem. Soc., Dalton Trans.* **1993**, 725.
(28) Lagrenée, M.; Sueur, S.; Wignacourt, J. P. *Acta Crystallogr.* **1991**, *C47*, 1158.
(29) Mangia, A.; Pelizzi, C.; Pelizzi, G. *Acta Crystallogr.* **1974**, *B30*, 2146.
(30) van Koningsbruggen, P. J.; Müller, E.; Haasnoot, J. G.; Reedijk, J. *Inorg. Chim. Acta* **1993**, *208*, 37.

Experimental Section

Physical Measurements. Electronic spectra were recorded as Nujol mulls and in solution using a Cary 5E spectrometer. Infrared spectra were recorded as Nujol mulls using a Mattson Polaris FT-IR instrument.

Mass spectra were obtained using a VG Micromass 7070HS spectrometer. Microanalyses were carried out by the Canadian Microanalytical Service, Delta, Canada. Room-temperature magnetic susceptibilities were measured by the Faraday method using a Cahn 7600 Faraday magnetic balance, and variable-temperature magnetic data (4−305 K) were obtained using an Oxford Instruments superconducting Faraday susceptometer with a Sartorius 4432 microbalance. A main solenoid field of 1.5 T and a gradient field of 10 T m^{-1} were employed. Calibrations were carried out with $HgCo(NCS)_4$, and temperature errors were determined with [TMEN][$CuCl_4$] (TMEN = $(CH_3)_2HNCH_2CH_2NH(CH_3)_2^{2+}$). The magnetic measurements were carried out on the same uniform samples that were analyzed structurally.

Syntheses. (a) PAHAP (1). PAHAP was prepared by a procedure different from that reported in the literature,[20] with an improved yield.

2-Cyanopyridine (20.8 g, 0.20 mol) was reacted with a solution of sodium methoxide, generated by addition of sodium metal (0.46 g, 0.020 mol) to dry methanol (200 mL), at room temperature for 12 h to yield the methyl ester of iminopicolinic acid.[30] Picolinamide hydrazone[31] (27.2 g, 0.20 mol) was added to the solution of iminopicolinic acid ester in situ, and the mixture was refluxed for 24 h. Cooling to room temperature produced yellow crystals (yield 40.8 g, 85%), which were recrystallized from ethanol (mp 210 °C; lit. 210−211 °C).

(b) PMHAP (2). Picolinamide hydrazone[31] (13.6 g, 0.100 mol) was reacted with 2-acetyl pyridine (12.1 g, 0.100 mol) in boiling absolute ethanol (50 mL) for 4 h. The resulting solution was cooled to room temperature, whereupon a yellow crystalline product was obtained (yield 17.9 g, 80%) (mp 117−118 °C). Mass spectrum (major mass peaks; *m*/*z*): 239 (M), 224 (M − CH_3), 161, 133, 108, 78. IR: ν_{CN} 1613 cm^{-1}, ν_{NH} 3465, 3318 cm^{-1}. Anal. Calcd for $C_{13}H_{13}N_5$: C, 65.26; H, 5.48; N, 29.27. Found: C, 65.26; H, 5.48; N, 29.42.

(c) [Cu_2(PAHAP)Cl_4]·H_2O (3), [Cu_2(PAHAP)Cl_4] (4), [Cu_2(PAHAP)Br_4]·H_2O (5), [Cu_2(PAHAP)$(H_2O)_6$]$(NO_3)_4$ (6), and [Cu_2(PAHAP-H)$(N_3)_2(NO_3)$] (7). PAHAP (0.24 g, 1.0 mmol) was added to an aqueous solution (30 mL) of $CuCl_2$·$2H_2O$ (0.34 g, 2.0 mmol), and the mixture was stirred for several minutes at room temperature until the ligand dissolved. The deep green solution was filtered, and the filtrate was allowed to stand at room temperature for several days. Dark green crystals, suitable for an X-ray structural determination, formed; these were filtered off, washed quickly with water, and air-dried (yield 90%). Anal. Calcd for [$Cu_2(C_{12}H_{12}N_6)Cl_4$]·$H_2O$ (**3**): C, 27.34; H, 2.68; N, 15.94. Found: C, 27.45; H, 2.63; N, 16.12. **6** was prepared in a similar manner using copper nitrate (yield 80%), forming crystals suitable for X-ray structural determination. Anal. Calcd for [$Cu_2(C_{12}H_{12}N_6)(H_2O)_{5.5}$]$(NO_3)_4$ (**6**): C, 20.17; H, 3.24; N, 19.60. Found: C, 20.22; H, 3.03; N, 19.46. The X-ray sample, which was not vacuum-dried, was shown to have four strongly and two weakly coordinated water molecules. **4** was prepared similarly to **3**, with the exception that a 2-fold excess of copper chloride was used. The complex was obtained as brown crystals (yield 92%). Anal. Calcd for [$Cu_2(C_{12}H_{12}N_6)Cl_4$] (**4**): C, 28.31; H, 2.37; N, 16.50. Found: C, 28.37; H, 2.38; N, 16.57. **5** was also prepared similarly to **3**, using copper(II) bromide, and was obtained as brown crystals. Anal. Calcd for [$Cu_2(C_{12}H_{12}N_6)Br_4$]·$H_2O$ (**5**): C, 20.44; H, 2.00; N, 11.92. Found: C, 20.55; H, 1.98; N, 11.92. **7** was prepared by addition of an aqueous solution of sodium azide to an aqueous solution of **6** and was obtained as olive green micro crystals. Anal. Calcd for [$Cu_2(C_{12}H_{11}N_6)(N_3)_2(NO_3)$] (**7**); C, 28.07; H, 2.14; N, 35.45. Found: C, 28.19; H, 2,18; N, 36.04.

(d) [Cu_2(PMHAP-H)$(NO_3)_3$] (8). A hot solution of PMHAP (0.240 g, 1.0 mmol) in dichloromethane (10 mL) was added to a hot solution of $Cu(NO_3)_2$·$3H_2O$ (0.60, 2.5 mmol) in methanol (20 mL), and the resulting solution was allowed to stand at room temperature overnight. Dark green crystals formed, which were suitable for X-ray structure determination (yield 0.45 g, 81%). Anal. Calcd for [$Cu_2(C_{13}H_{12}N_5)(NO_3)_3$] (**8**): C, 28.32; H, 2.19; N, 20.32. Found: C, 28.30; H, 2.31; N, 20.29.

(31) Case, F. H. *J. Org. Chem.* **1965**, *30*, 931.

Crystallographic Data Collection and Refinement of the Structures. (a) PAHAP (1). The crystals of **1** are yellow. The diffraction intensities of an approximately 0.35 × 0.25 × 0.40 mm crystal were collected with graphite-monochromatized Mo Kα radiation using a Rigaku AFC6S diffractometer at 26 ± 1 °C and the ω-2θ scan technique to a $2\theta_{max}$ value of 50.1°. A total of 2533 reflections were measured, and 1229 were considered significant with $I_{net} > 2.0\sigma(I_{net})$. The intensities of three representative reflections, which were measured after every 150 reflections, remained constant throughout the data collection, indicating crystal and electronic stability (no decay correction was applied). An empirical absorption correction, based on azimuthal scans of several reflections, was applied, which resulted in transmission factors ranging from 0.97 to 1.00. The data were corrected for Lorentz and polarization effects. The cell parameters were obtained from the least-squares refinement of the setting angles of 23 carefully centered reflections with 2θ in the range 20.1−26.3°.

The structure was solved by direct methods.[32,33] All atoms except hydrogens were refined anisotropically. Hydrogen atoms were optimized by positional refinement, with isotropic thermal parameters set 20% greater than those of their bonded partners at the time of their inclusion. However, they were fixed for the final round of refinement. The final cycle of full-matrix least-squares refinement was based on 1229 observed reflections ($I > 2.00\sigma$(I)) and 164 variable parameters and converged with unweighted and weighted agreement factors of $R = \sum||F_o| - |F_c||/\sum|F_o| = 0.045$ and $R_w = [(\sum w(|F_o| - |F_c|)^2/\sum wF_o^2)]^{1/2} = 0.038$. The maximum and minimum peaks on the final difference Fourier map correspond to 0.14 and −0.19 electron $Å^{-3}$, respectively. Neutral-atom scattering factors[34] and anomalous-dispersion terms[35,36] were taken from the usual sources. All calculations were performed with the TEXSAN[37] crystallographic software package using a VAX 3100 work station. Abbreviated crystal data are given in Table 1, and significant atomic positional parameters, in Table 2. Listings of complete experimental and crystal data (Table S1), atomic positional parameters (Table S2), anisotropic thermal parameters (Table S3), and complete bond distances and angles (Table S4) are included as Supporting Information.

(b) [Cu_2(PAHAP)Cl_4]·H_2O (3), [Cu_2(PAHAP)Br_4]·H_2O (5), and [Cu_2(PAHAP)$(H_2O)_6$]$(NO_3)_4$ (6). The data collections and structure solutions were carried out in a manner similar to that for **1**. Abbreviated crystal data are given in Table 1, and significant atomic positional parameters, in Tables 3−5, respectively. Listings of complete experimental and crystal data (Table S1), atomic positional parameters (Tables S5, S8, and S11, respectively), anisotropic thermal parameters (Tables S6, S9, and S12, respectively), and complete bond distances and angles (Tables S7, S10, and S13, respectively) are included as Supporting Information. Bromine Br(3) in **5** exhibited some positional disorder and was modeled with two (80/20) components. Only one hydrogen associated with the lattice water molecule could be found in difference maps.

(c) [Cu_2(PMHAP-H)$(NO_3)_3$] (8). The crystals of **8** are green. A single crystal of **8** of dimensions 0.20 × 0.10 × 0.10 mm was attached to a quartz fiber and transferred to a Siemens SMART three-circle diffractometer using graphite-monochromatized Mo Kα radiation, equipped with a CCD area detector, and controlled by a Pentium-based PC running the SMART software package.[38] ω-scans were used in such a way that an initial 180° scan range consisting of 0.3° intervals is followed by three further 120, 180, and 120° scans with ϕ offsets of 88, 180, and 268°, respectively. This strategy samples the sphere of reciprocal space up to $2\theta = 56.62°$. Cell parameters were refined using the centroid values of 300 reflections with 2θ angles up to 56.62°.

(32) Gilmore, C. J. *J. Appl. Crystallogr.* **1984**, *17*, 42.
(33) Beurskens, P. T. *DIRDIF*; Technical Report 1984/1; Crystallography Laboratory: Toernooiveld, 6525 Ed Nijmegen, The Netherlands, 1984.
(34) Cromer, D. T.; Waber, J. T. *International Tables for X-ray Crystallography*; The Kynoch Press: Birmingham, U.K., 1974; Vol. IV, Table 2.2A.
(35) Ibers, J. A.; Hamilton, W. C. *Acta Crystallogr.* **1964**, *17*, 781.
(36) Cromer, D. T. *International Tables for X-ray Crystallography*; The Kynoch Press: Birmingham, U.K., 1974; Vol. IV, Table 2.3.1.
(37) *Texsan-Texray Structure Analysis Package*; Molecular Structure Corp.: The Woodlands, TX, 1985.
(38) *SMART*: *Data Collection Software*, Version 4.050; Siemens Analytical X-ray Instruments Inc.: Madison, WI, 1996.

Table 1. Summary of Crystallographic Data for PAHAP (**1**), $[Cu_2(PAHAP)Cl_4]\cdot H_2O$ (**3**), $[Cu_2(PAHAP)Br_4]\cdot H_2O$ (**5**), $[Cu_2(PAHAP)(H_2O)_6](NO_3)_4$ (**6**), and $[Cu_2(PMHAP\text{-}H)(NO_3)_3]$ (**8**)

	1	**3**	**5**	**6**	**8**[c]
empirical formula	$C_{12}H_{12}N_6$	$C_{12}H_{14}N_6OCl_4Cu_2$	$C_{12}H_{13}N_6OBr_4Cu_2$	$C_{12}H_{24}N_{10}O_{18}Cu_2$	$C_{13}H_{12}N_8O_9Cu_2$
fw	240.27	527.19	703.98	723.47	551.39
space group	*Pbca* (No. 61)	*C*2/*c* (No. 15)	*C*2/*c* (No. 15)	*C*2/*c* (No. 15)	$P\bar{1}$
a (Å)	19.845(4)	26.732(6)	27.336(2)	20.983(4)	7.838(1)
b (Å)	13.178(5)	8.670(9)	8.859(4)	7.505(4)	8.015(3)
c (Å)	9.483(8)	16.436(4)	16.795(3)	17.219(3)	15.655(4)
α (deg)					99.81(3)
β (deg)		100.88(2)	100.78(1)	104.22(1)	101.74(2)
γ (deg)					94.52(2)
V (Å^3)	2480(4)	3741(6)	3996(3)	2628(1)	942.2(4)
ρ_{calcd} (g cm^{-3})	1.287	1.872	2.340	1.828	1.943
Z	8	8	8	4	2
μ (cm^{-1})	0.79	28.72	100.75	17.18	23.28
λ (Å)	0.710 69	0.710 69	0.710 69	0.710 69	0.710 73
T, K	299(1)	299(1)	299(1)	299(1)	298(2)
R^a	0.045	0.029	0.037	0.048	$R_1 = 0.0708$
$R_w{}^b$	0.038	0.025	0.030	0.053	w$R_2 = 0.1563$

[a] $R = \sum||F_o| - |F_c||/\sum|F_o|$. [b] $R_w = [\sum w(|F_o| - |F_c|)^2/\sum wF_o^2]^{1/2}$. [c] Siemens Smart data. $R_1 = \sum||F_o| - ||F_c||/\sum|F_o|$. w$R_2 = [\sum w(|F_o|^2 - |F_c|^2)^2/\sum w(|F_o|^2)^2]^{1/2}$.

Table 2. Final Atomic Positional Parameters and B_{eq} Values (Å^2) for Significant Atoms in PAHAP (**1**)

atom	*x*	*y*	*z*	$B_{eq}{}^a$
N(1)	0.6933(1)	0.6148(2)	0.3731(3)	4.8(1)
N(2)	0.5894(1)	0.4899(2)	0.3382(3)	4.9(1)
N(3)	0.6152(1)	0.4091(2)	0.5517(2)	3.2(1)
N(4)	0.5596(1)	0.3460(2)	0.5151(2)	3.3(1)
N(5)	0.5773(1)	0.2764(2)	0.7395(3)	4.2(1)
N(6)	0.4834(1)	0.1330(2)	0.6760(3)	4.5(1)
C(1)	0.7439(2)	0.6801(3)	0.3912(4)	6.1(2)
C(2)	0.7851(2)	0.6837(3)	0.5069(4)	5.3(2)
C(3)	0.7741(2)	0.6142(3)	0.6126(4)	4.8(2)
C(4)	0.7222(2)	0.5452(2)	0.5988(3)	3.9(2)
C(5)	0.6830(1)	0.5483(2)	0.4778(3)	3.4(1)
C(6)	0.6255(2)	0.4769(2)	0.4565(3)	3.2(1)
C(7)	0.5446(1)	0.2832(2)	0.6154(3)	3.0(1)
C(8)	0.4871(1)	0.2137(2)	0.5909(3)	3.2(1)
C(9)	0.4405(1)	0.2327(2)	0.4864(4)	4.2(2)
C(10)	0.3879(2)	0.1658(3)	0.4671(4)	5.5(2)
C(11)	0.3836(2)	0.0843(3)	0.5523(4)	6.6(2)
C(12)	0.4313(2)	0.0699(3)	0.6556(4)	6.3(2)

[a] $B_{eq} = (8\pi^2/3)\sum^3_{i=1}\sum^3_{j=1}U_{ij}\vec{a}_i^*\vec{a}_j^*\vec{a}_i\cdot\vec{a}_j$.

Raw frame data were integrated using the SAINT program.[39] The structure was solved by direct methods.[40] An empirical absorption correction was applied to the data using the program SADABS.[41]

Abbreviated crystal data are given in Table 1, and significant atomic positional parameters are given in Table 6. Listings of complete experimental and crystal data (Table S1), atomic positional parameters (Table S14), anisotropic thermal parameters (Tables S15), and complete bond distances and angles (Tables S16) are included as Supporting Information.

Results and Discussion

Structures. (a) PAHAP (1). The structure of **1** is illustrated in Figure 3, and relevant bond distances and angles are listed in Table 7. The molecule is essentially flat and has a *trans* configuration. The dihedral angle between the least-squares planes including the atom groups N(1)−C(5)−C(6)−N(2)−N(3) and N(6)−C(8)−C(7)−N(5)−N(4) is 6.2°. The nitrogen−nitrogen bond N(3)−N(4) (1.424(3) Å) can be formally defined as a single bond and compares closely with the N−N bond distance in hydrazine (1.47 Å). The C−N bonds C(6)−N(3) and C(7)−N(4) (1.287(3) and 1.295(3) Å, respectively) are considered to have full double-bond character. Intramolecular contacts between the amine hydrogen atoms attached to N(2) and N(5) and adjacent sp^2 nitrogens N(1), N(4) and N(3), N(6), respectively, are too long to be considered as hydrogen bonds. The overall *trans* configuration is therefore due mainly to steric repulsion effects. An examination of intermolecular contacts reveals only two of possible significance between N(4) and N(6) and hydrogens bonded to N(5)′ and N(2)′, respectively (N−H = 2.183 and 2.179 Å, respectively), but these are clearly weak.

Table 3. Final Atomic Positional Parameters and B_{eq} Values (Å^2) for Significant Atoms in $[Cu_2(PAHAP)Cl_4]\cdot H_2O$ (**3**)

atom	*x*	*y*	*z*	$B_{eq}{}^a$
Cu(1)	0.05293(2)	0.49854(6)	0.09348(3)	2.55(2)
Cu(2)	0.19512(2)	0.52887(6)	0.19090(3)	2.37(2)
Cl(1)	−0.01685(4)	0.6455(1)	0.07789(7)	3.86(5)
Cl(2)	0.10519(4)	0.6991(1)	0.08321(7)	3.69(5)
Cl(3)	0.14538(4)	0.4588(1)	0.28140(6)	3.01(4)
Cl(4)	0.23500(4)	0.7177(1)	0.27392(6)	3.47(5)
O(1)	0.3775(1)	0.3643(4)	0.2220(2)	5.6(2)
N(1)	0.0186(1)	0.3095(4)	0.1303(2)	2.4(1)
N(2)	0.1086(1)	0.3457(3)	0.0983(2)	2.0(1)
N(3)	0.1601(1)	0.3877(3)	0.1026(2)	1.9(1)
N(4)	0.2405(1)	0.5544(3)	0.1060(2)	2.2(1)
N(5)	0.1367(1)	0.1100(4)	0.1604(2)	3.0(1)
N(6)	0.1449(1)	0.3681(4)	−0.0417(2)	3.2(2)
C(1)	−0.0299(1)	0.2955(5)	0.1396(3)	3.3(2)
C(2)	−0.0512(1)	0.1540(5)	0.1500(3)	3.7(2)
C(3)	−0.0236(2)	0.0230(5)	0.1470(3)	3.8(2)
C(4)	0.0269(1)	0.0357(5)	0.1379(3)	3.1(2)
C(5)	0.0467(1)	0.1799(4)	0.1329(2)	2.2(2)
C(6)	0.1012(1)	0.2117(4)	0.1302(2)	2.1(2)
C(7)	0.1730(1)	0.4068(4)	0.0306(2)	2.1(2)
C(8)	0.2230(1)	0.4816(4)	0.0337(2)	2.1(1)
C(9)	0.2489(1)	0.4838(5)	−0.0310(2)	3.1(2)
C(10)	0.2937(1)	0.5675(5)	−0.0218(3)	3.6(2)
C(11)	0.3110(1)	0.6438(5)	0.0503(3)	3.3(2)
C(12)	0.2839(1)	0.6329(5)	0.1138(2)	2.9(2)

[a] $B_{eq} = (8\pi^2/3)\sum^3_{i=1}\sum^3_{j=1}U_{ij}\vec{a}_i^*\vec{a}_j^*\vec{a}_i\cdot\vec{a}_j$.

(b) $[Cu_2(PAHAP)Cl_4]\cdot H_2O$ (3). The structure of **3** is illustrated in Figure 4, and relevant bond distances and angles are listed in Table 8. Two copper(II) ions are bound to one PAHAP ligand each via a pyridine and a diazine nitrogen in a twisted structure, with nominal four-coordination being completed at each copper center by two chlorines. Cu−N and Cu−

(39) *SAINT*: *Data Reduction Software*, Version 4.050; Siemens Analytical X-ray Instruments Inc.: Madison, WI, 1996.
(40) Sheldrick, G. M. *SHELXTL 5.04/VMS*: *An integrated system for solving, refining and displaying crystal structures from diffraction data*; Siemens Analytical X-ray Instruments Inc.: Madison, WI, 1995.
(41) Sheldrick, G. M. *SADABS: Empirical Absorption Correction Program*; University of Göttingen: Göttingen, Germany, 1996.

Table 4. Final Atomic Positional Parameters and B_{eq} Values (Å^2) for Significant Atoms in $[Cu_2(PAHAP)Br_4]\cdot H_2O$ (**5**)

atom	*x*	*y*	*z*	B_{eq}[a]
Br(1)	0.26659(3)	0.7310(1)	0.22508(5)	3.78(4)
Br(2)	0.35820(3)	0.4613(1)	0.21509(4)	3.37(4)
Br(3A)	0.5167(1)	0.6573(5)	0.4212(2)	3.78(7)
Br(3B)	0.5146(6)	0.662(2)	0.395(1)	9.6(8)
Br(4)	0.39244(3)	0.7090(1)	0.42050(5)	3.87(4)
Cu(1)	0.30714(3)	0.5333(1)	0.31067(5)	2.63(4)
Cu(2)	0.44558(3)	0.5007(1)	0.40374(5)	2.93(4)
O(1)	0.3811(2)	0.1236(7)	0.7210(4)	6.6(4)
N(1)	0.2626(2)	0.5533(6)	0.3938(3)	2.1(2)
N(2)	0.3409(2)	0.3906(6)	0.3950(3)	2.0(2)
N(3)	0.3914(2)	0.3492(6)	0.3993(3)	2.4(3)
N(4)	0.4797(2)	0.3162(6)	0.3693(3)	2.5(3)
N(5)	0.3544(2)	0.3594(7)	0.5357(3)	3.6(3)
N(6)	0.3649(2)	0.1174(7)	0.3406(4)	3.5(3)
C(1)	0.2196(3)	0.6294(9)	0.3871(4)	3.3(4)
C(2)	0.1923(3)	0.634(1)	0.4484(5)	3.9(4)
C(3)	0.2093(3)	0.555(1)	0.5178(5)	4.1(4)
C(4)	0.2532(3)	0.474(1)	0.5258(4)	3.5(4)
C(5)	0.2789(2)	0.4782(8)	0.4626(4)	2.4(3)
C(6)	0.3275(2)	0.4038(8)	0.4649(4)	2.4(3)
C(7)	0.3995(2)	0.2207(8)	0.3692(4)	2.4(3)
C(8)	0.4521(2)	0.1906(8)	0.3652(4)	2.5(3)
C(9)	0.4716(3)	0.0480(9)	0.3591(5)	3.8(4)
C(10)	0.5216(3)	0.039(1)	0.3512(5)	4.5(4)
C(11)	0.5484(3)	0.166(1)	0.3514(5)	4.0(4)
C(12)	0.5271(3)	0.304(1)	0.3601(5)	3.6(4)

[a] $B_{eq} = (8\pi^2/3)\sum_{i=1}^{3}\sum_{j=1}^{3}U_{ij}\boldsymbol{a}_i^*\boldsymbol{a}_j^*\vec{\boldsymbol{a}}_i\cdot\vec{\boldsymbol{a}}_j$.

Table 5. Final Atomic Positional Parameters and B_{eq} Values (Å^2) for Significant Atoms in $[Cu_2(PAHAP)(H_2O)_6](NO_3)_4$ (**6**)

atom	*x*	*y*	*z*	B_{eq}[a]
Cu(1)	0.89212(3)	−0.8144(1)	0.21512(4)	2.40(3)
O(1)	0.8071(2)	−0.7006(6)	0.2080(3)	3.1(2)
O(2)	0.9313(2)	−0.6974(6)	0.3189(2)	3.4(2)
N(1)	0.8631(2)	−0.9413(7)	0.1102(3)	2.4(2)
N(2)	0.9706(2)	−0.9565(6)	0.2184(3)	2.1(2)
N(3)	1.0229(2)	−1.1366(8)	0.1441(3)	4.0(3)
C(1)	0.8035(3)	−0.935(1)	0.0590(4)	3.5(3)
C(2)	0.7916(3)	−1.019(1)	−0.0146(4)	4.4(3)
C(3)	0.8406(4)	−1.108(1)	−0.0367(4)	4.8(4)
C(4)	0.9021(3)	−1.118(1)	0.0164(4)	3.7(3)
C(5)	0.9107(3)	−1.0348(8)	0.0899(3)	2.5(2)
C(6)	0.9729(3)	−1.0444(8)	0.1546(3)	2.2(2)

[a] $B_{eq} = (8\pi^2/3)\sum_{i=1}^{3}\sum_{j=1}^{3}U_{ij}\boldsymbol{a}_i^*\boldsymbol{a}_j^*\vec{\boldsymbol{a}}_i\cdot\vec{\boldsymbol{a}}_j$.

Cl distances are normal for equatorial coordination to copper(II). The diazine nitrogen bond distance N(2)−N(3) is 1.411(4) Å, implying single-bond character, and is largely unchanged from that of the free ligand. The C=N bonds (C(6)−N(2) and C(7)−N(3); 1.305(4) and 1.304(4) Å, respectively) are essentially the same as those in PAHAP. However the sums of the angles at N(2) and N(3) (354.7, and 349.7°, respectively) imply slight pyramidal distortion at these centers.

The two copper planes do not adopt a *trans* conformation about the N−N bond, as might have been expected, but instead adopt a folded *cis* conformation with an acute angle between the planes. Molecular models suggest that a *trans* structure would be unlikely because of steric constraints associated with the terminal chlorines and the amine groups. One significant factor responsible for the acute folding is considered to be a long intramolecular axial contact between Cu(2) and Cl(2) (3.080(3) Å), which effectively locks the two copper planes in place, creating a square-pyramidal geometry at Cu(2) (Figure 4). An analysis of intermolecular contacts reveals that two molecules are effectively joined together via a long axial contact between Cu(1) and Cl(1) (3.066 Å) on an adjacent molecule, so that the complex is in reality a weakly associated dimer. The twist of the copper CuN_2Cl_2 planes can best be visualized in terms of the 77.1° dihedral angle between the planes Cu(1)−N(1)−C(5)−C(6)−N(2) and Cu(2)−N(4)−C(8)−C(7)−N(3). The resulting copper−copper separation (3.845(1) Å) is quite long, as would be expected. The lattice water molecule is not involved in coordination to copper and does not take part in any significant hydrogen-bonding interactions. It can be concluded therefore that the molecular twist in **3** is the result of a balance between steric factors, principally associated with the chlorines and NH_2 groups on the ligand, and the weak axial interaction between Cu(2) and Cl(2).

Table 6. Final Atomic Coordinates ($\times 10^4$) and Equivalent Isotropic Displacement Parameters (Å^2 $\times$ 10^3) for Significant Atoms in $[Cu_2(PMHAP\text{-}H)(NO_3)_3]$ (**8**)

atom	*x*	*y*	*z*	U_{eq}[a]
Cu(1)	9467(1)	1399(1)	3018(1)	35(1)
Cu(2)	13247(1)	6144(1)	2725(1)	36(1)
N(1)	8317(6)	249(6)	1801(3)	36(1)
N(2)	10381(6)	3028(5)	2382(3)	31(1)
N(3)	10661(6)	3135(6)	4005(3)	38(1)
N(4)	11460(5)	4447(6)	2904(3)	33(1)
N(5)	13797(6)	6674(5)	4034(3)	33(1)
N(6)	9571(6)	−1266(6)	3802(3)	40(1)
N(7)	13167(8)	9063(7)	2120(3)	49(1)
N(8)	15404(7)	4621(6)	1823(4)	45(1)
O(1)	8437(5)	−202(5)	3671(3)	45(1)
O(2)	9276(7)	−2433(6)	4174(3)	65(1)
O(3)	10893(6)	−1048(6)	3508(4)	68(1)
O(4)	14280(6)	8428(5)	2662(3)	50(1)
O(5)	13502(9)	10547(7)	2056(4)	88(2)
O(6)	11842(7)	8127(7)	1692(3)	66(1)
O(7)	13822(5)	4969(6)	1610(3)	49(1)
O(8)	16092(6)	3955(7)	1246(3)	69(1)
O(9)	16151(6)	5007(7)	2617(3)	67(1)
C(1)	7374(8)	−1269(8)	1538(4)	48(2)
C(2)	6699(9)	−1954(9)	658(5)	59(2)
C(3)	7012(9)	−1043(8)	19(4)	54(2)
C(4)	8003(8)	545(8)	281(4)	46(1)
C(5)	8644(7)	1161(7)	1181(4)	36(1)
C(6)	9737(6)	2846(7)	1542(4)	34(1)
C(7)	9936(8)	4104(8)	964(4)	44(1)
C(8)	15068(7)	7848(7)	4553(4)	39(1)
C(9)	15326(8)	8150(7)	5464(4)	41(1)
C(10)	14289(8)	7203(8)	5855(4)	44(1)
C(11)	13026(7)	5935(7)	5328(4)	37(1)
C(12)	12811(6)	5709(6)	4415(3)	30(1)
C(13)	11556(7)	4352(6)	3771(3)	31(1)

[a] U_{eq} is defined as one-third of the trace of the orthogonalized $\mathbf{U}_{ij}$ tensor.

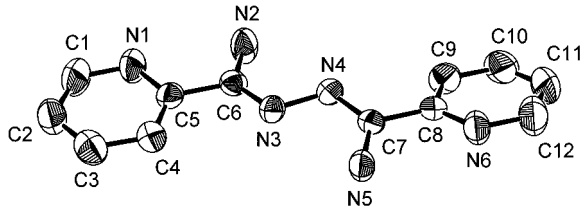

Figure 3. Structural representation of PAHAP (**1**) with hydrogen atoms omitted (40% probability thermal ellipsoids).

Table 7. Interatomic Distances (Å) and Angles (deg) for PAHAP (**1**)

N(2)−C(6)	1.343(4)	N(3)−N(4)	1.424(3)
N(3)−C(6)	1.287(3)	N(4)−C(7)	1.295(3)
N(5)−C(7)	1.347(4)		
N(2)−C(6)−C(5)	116.1(3)	N(4)−N(3)−C(6)	110.9(2)
N(3)−C(6)−C(5)	117.7(3)	N(3)−N(4)−C(7)	111.9(2)
N(4)−C(7)−N(5)	124.9(3)	N(4)−C(7)−C(8)	117.2(3)
N(5)−C(7)−C(8)	117.8(3)	N(2)−C(6)−N(3)	126.2(3)

(c) $[Cu_2(PAHAP)Br_4]\cdot H_2O$ (5). The structure of **5** is illustrated in Figure 5, and relevant bond distances and angles

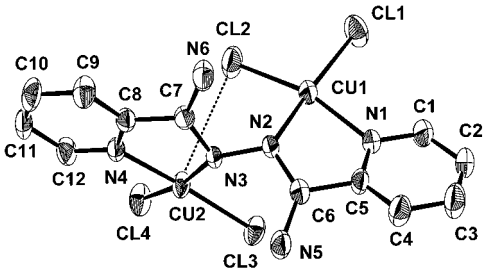

Figure 4. Structural representation of $[Cu_2(PAHAP)Cl_4]\cdot H_2O$ (**3**) with hydrogen atoms omitted (40% probability thermal ellipsoids).

Table 8. Interatomic Distances (Å) and Angles (deg) Relevant to the Copper Coordination Spheres and the Ligand in $[Cu_2(PAHAP)Cl_4]\cdot H_2O$ (**3**)

Cu(1)−Cl(1)	2.233(1)	Cu(2)−Cl(3)	2.258(1)
Cu(1)−Cl(2)	2.257(2)	Cu(2)−Cl(4)	2.265(2)
Cu(1)−N(1)	2.027(3)	Cu(2)−N(3)	1.992(3)
Cu(1)−N(2)	1.984(3)	Cu(2)−N(4)	2.026(3)
N(5)−C(6)	1.321(4)	N(6)−C(7)	1.323(4)
C(5)−C(6)	1.493(5)	C(7)−C(8)	1.479(5)
N(2)−N(3)	1.411(4)	N(2)−C(6)	1.305(4)
N(3)−C(7)	1.304(4)	Cu(1−Cu(2)	3.845(1)
Cl(1)−Cu(1)−Cl(2)	93.85(7)	Cl(3)−Cu(2)−Cl(4)	93.82(5)
Cl(1)−Cu(1)−N(1)	94.6(1)	Cl(3)−Cu(2)−N(3)	93.44(9)
Cl(1)−Cu(1)−N(2)	171.91(9)	Cl(3)−Cu(2)−N(4)	170.62(9)
Cl(2)−Cu(1)−N(1)	165.32(9)	Cl(4)−Cu(2)−N(3)	170.45(9)
Cl(2)−Cu(1)−N(2)	92.7(1)	Cl(4)−Cu(2)−N(4)	93.52(9)
N(1)−Cu(1)−N(2)	80.0(1)	N(3)−Cu(2)−N(4)	80.0(1)
N(2)−C(6)−N(5)	126.3(3)	N(2)−C(6)−C(5)	113.6(3)
N(5)−C(6)−C(5)	120.1(3)	N(3)−C(7)−N(6)	125.5(3)
N(3)−C(7)−C(8)	114.7(3)	N(6)−C(7)−C(8)	119.8(3)
N(3)−N(2)−C(6)	115.5(3)	N(2)−N(3)−C(7)	114.2(3)
Cu(1)−N(2)−N(3)	123.1(2)	Cu(1)−N(2)−C(6)	116.1(2)
Cu(2)−N(3)−N(2)	121.0(2)	Cu(2)−N(3)−C(7)	114.5(2)

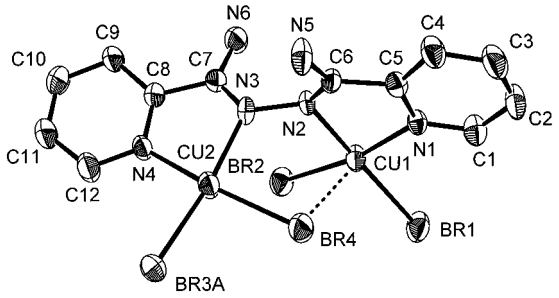

Figure 5. Structural representation of $[Cu_2(PAHAP)Br_4]\cdot H_2O$ (**5**) with hydrogen atoms and Br(3B) omitted (40% probability thermal ellipsoids).

Table 9. Interatomic Distances (Å) and Angles (deg) Relevant to the Copper Coordination Spheres and the Ligand in $[Cu_2(PAHAP)Br_4]\cdot H_2O$ (**5**)

Br(1)−Cu(1)	2.401(1)	N(5)−C(6)	1.334(8)
Br(2)−Cu(1)	2.402(1)	N(6)−C(7)	1.339(8)
Br(3A)−Cu(2)	2.362(4)	N(2)−N(3)	1.416(6)
Br(3B)−Cu(2)	2.39(2)	N(2)−C(6)	1.298(8)
Br(4)−Cu(2)	2.398(1)	N(3)−C(7)	1.282(8)
Cu(1)−N(1)	2.025(5)	Cu(1)−Cu(2)	3.826(1)
Cu(1)−N(2)	1.992(5)	Cu(2)−N(3)	1.991(6)
Cu(2)−N(4)	2.020(6)		
Br(1)−Cu(1)−Br(2)	93.12(4)	Br(1)−Cu(1)−N(1)	94.5(2)
Br(1)−Cu(1)−N(2)	171.6(2)	Br(2)−Cu(1)−N(1)	169.6(2)
Br(2)−Cu(1)−N(2)	93.3(1)	N(1)−Cu(1)−N(2)	79.9(2)
Br(3A)−Cu(2)−Br(4)	92.1(1)	Br(3A)−Cu(2)−N(3)	172.2(2)
Br(3A)−Cu(2)−N(4)	95.6(2)	Br(4)−Cu(2)−N(3)	93.4(2)
Br(4)−Cu(2)−N(4)	168.3(2)	N(3)−Cu(2)−N(4)	79.9(2)

are listed in Table 9. The structure is very similar to that of **3**, with two essentially planar copper(II) centers bound in a twisted *cis* conformation. Deviations of the atoms in the N_2Br_2 donor sets are <0.24 Å from their least-squares planes, with Cu(1) displaced by 0.0160 Å and Cu(2) displaced by 0.0364 Å from their respective planes. The fold angle between the copper planes, as defined by the two CuN_2C_2 chelate rings, is 75.02°, in close agreement with that in **3**. Cu−N distances are normal, and Cu−Br distances are close to 2.4 Å. The Cu−Cu separation (3.826(1) Å) is almost identical to that in **3**. The Cu(1)−Br(4) distance (3.107(1) Å) is very close to the intramolecular chlorine bridging contact in **3**, and so it is reasonable to assume a similar bridging situation in **5**. The Cu(2)−Br(2) distance (3.611(1) Å) is much to long for a second bridge. Intermolecular contacts involving potential bromine bridges are also too long to be significant (>3.24 Å), and so **5** is considered to be an essentially isolated dinuclear species. The similarity in fold angles for **3** and **5** is considered to result from the similar weak halogen-bridged structural arrangement. Br(3) was modeled as two components in a disordered situation with an 80/20 composition. The residual electron density close to Br(3A) could not be sensibly accounted for in any other way.

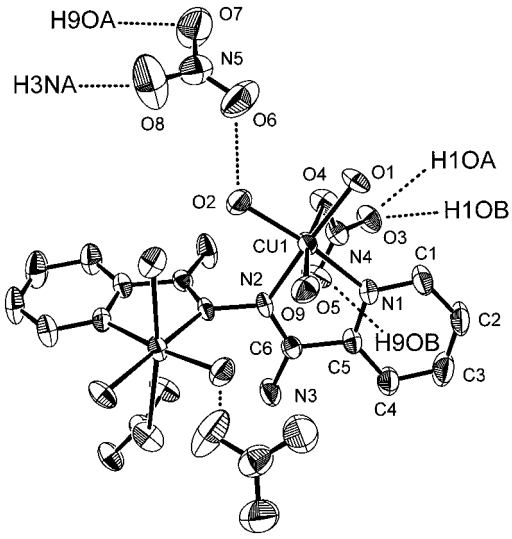

Figure 6. Structural representation of $[Cu_2(PAHAP)(H_2O)_6](NO_3)_4$ (**6**) with hydrogen atoms omitted (40% probability thermal ellipsoids). Significant hydrogen-bonding contacts are shown (dotted lines).

Table 10. Interatomic Distances (Å) and Angles (deg) Relevant to the Copper Coordination Spheres and the Ligand in $[Cu_2(PAHAP)(H_2O)_6](NO_3)_4$ (**6**)

Cu(1)−O(1)	1.954(4)	Cu(1)−N(1)	2.000(5)
Cu(1)−O(2)	1.980(4)	Cu(1)−N(2)	1.952(4)
Cu(1)−O(9)	2.392(5)	Cu(1)−O(4)	2.724(5)
C(5)−C(6)	1.495(7)	N(2)−N(2)	1.430(8)
N(2)−C(6)	1.292(7)	N(3)−C(6)	1.306(7)
Cu(1)−Cu(1)a	4.389(2)		
O(1)−Cu(1)−O(2)	91.9(2)	O(2)−Cu(1)−N(1)	173.4(2)
O(1)−Cu(1)−N(1)	94.6(2)	O(2)−Cu(1)−N(2)	93.2(2)
O(1)−Cu(1)−N(2)	172.6(2)	N(1)−Cu(1)−N(2)	80.4(2)
N(2)−C(6)−N(3)	125.9(5)	N(2)−C(6)−C(5)	113.7(5)
N(3)−C(6)−C(5)	120.4(5)	Cu(1)−N(2)−N(2)	125.8(4)
Cu(1)−N(2)−C(6)	117.5(4)	N(2)−N(2)−C(6)	116.3(5)

(d) $[Cu_2(PAHAP)(H_2O)_6](NO_3)_4$ (6). The structure of **6** is illustrated in Figure 6, and relevant bond distances and angles are listed in Table 10. The two distorted octahedral copper ions are bound to PAHAP in a manner similar to that in **3**, with a twisted arrangement of the copper basal planes about the N−N bond, which clearly has single-bond character (N(2)−N(2)′ 1.430(8) Å). The C═N bond lengths (C(6)−N(2) 1.292(7) Å) are the same as those in PAHAP, and sum of the angles at N(2) (359.6°) indicates that there is no pyramidal distortion at this donor center. Three water molecules are bound to each copper-

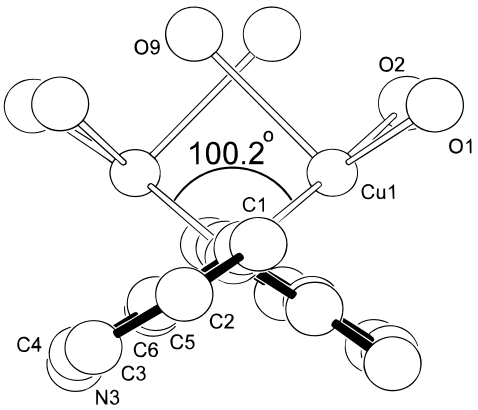

Figure 7. Structural representation of **6** viewed along an axis close to that of the N−N bond.

(II) ion, two with short contacts in the basal plane (Cu(1)−O(1) 1.954(4) Å; Cu(1)−O(2) 1.980(4) Å) and one in the axial position (Cu(1)−O(9) 2.392(5) Å). A much longer contact to a nitrate oxygen (Cu(1)−O(4) 2.724(5) Å) indicates that a nitrate is semicoordinated as a weak sixth ligand. The copper atom is displaced slightly from the mean N_2O_2 basal plane toward O(9) by 0.0367 Å.

The molecular twist in **6** about the N−N bond is substantially larger than that in **3** and **5**. The dihedral angle between the least-squares planes Cu(1)−N(2)−C(6)−C(5)−N(1) and Cu(1)a−N(2)a−C(6)a−C(5)a−N(1)a is 100.2°, indicating a significant opening of the complex along the N−N bond in comparison with the case of **3** and **5**. Figure 7 illustrates a projection of **6** viewed along the N−N bond. This gives a reasonable representation of the angle between the copper magnetic planes and explains why the Cu−Cu separation (4.389(2) Å) is so much larger than that in **3** and **5**. The most significant difference among **3**, **5**, and **6** rests with the different ligands in the copper equatorial plane and with the presence of an axial, nonbridging water ligand (O(9)) in **6**. Steric repulsions between the coordinated water molecules at each metal center, and also between the NH_2 groups, combined with the absence of a bridging ligand interaction, would reasonably allow the copper planes to move farther apart until a balance between these repulsive forces was achieved. However such an effect cannot necessarily be considered in isolation, and in this case, hydrogen-bonding interactions should also be taken into account. Several hydrogen-bonding contacts (X---H < 1.9 Å) have been identified (H(20A)−O(6) 1.824 Å, H(3NA)−O(8) 1.871 Å, H(90A)−O(7) 1.832 Å, H(90B)−O(5) 1.782 Å, H(10A)−O(3) 1.863 Å, H(10B)−O(3) 1.800 Å, H(3NA)−O(8) 1.871 Å), all of which have X---H---Y angles in the range 153−175°. These are illustrated in Figure 6. Nitrate N(5) is involved in the most contacts and provides significant links between the dinuclear complex ions through the shortest interaction (O(2)−O(6) 2.724(8)Å). Other contacts through O(7) and O(8) create further links within the lattice structure. Nitrate N(4) is also involved in intermolecular contacts to water molecules O(1) and O(9). These hydrogen-bonding interactions are possibly of significance in creating intermolecular spin exchange pathways (vide supra) but may also influence the twist between the copper equatorial coordination planes.

(e) [Cu_2(PMHAP-H)$(NO_3)_3$] (8). The structure of **8** is illustrated in Figure 8, and relevant bond distances and angles are listed in Table 11. The ligand PMHAP binds two copper centers in a *trans* structure and acts in a quinquedentate fashion with Cu(1) coordinated to pyridine (N(1)), diazine (N(2)), and amino (N(3)) nitrogens and with Cu(2) bound to diazine (N(4)) and pyridine (N(5)) nitrogens. The presence of only three

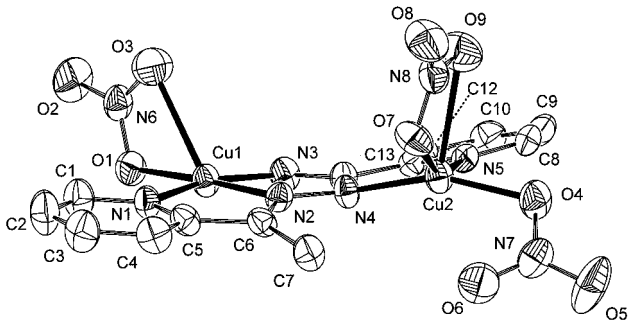

Figure 8. Structural representation of [Cu_2(PMHAP-H)$(NO_3)_3$] (**8**) with hydrogen atoms omitted (50% probability thermal ellipsoids).

Table 11. Interatomic Distances (Å) and Angles (deg) Relevant to the Copper Coordination Spheres and the Ligand in [Cu_2(PMHAP-H)$(NO_3)_3$] (**8**)

Cu(1−N(3)	1.916(5)	Cu(2)−O(7)	1.991(4)
Cu(1)−N(2)	1.948(4)	N(2)−C(6)	1.287(6)
Cu(1)−N(1)	1.966(5)	N(2)−N(4)	1.389(6)
Cu(1)−O(1)	1.990(4)	N(3)−C(13)	1.303(6)
Cu(2)−O(4)	1.968(4)	N(4)−C(13)	1.359(6)
Cu(2)−N(5)	1.970(4)	C(5)−C(6)	1.496(7)
Cu(2)−N(4)	1.971(4)	C(12)−C(13)	1.490(7)
Cu(1)−O(3)	2.489(4)	Cu(2)−O(9)	2.544(4)
Cu(1)−Cu(2)	4.778(4)		
N(3)−Cu(1)−N(2)	80.3(2)	N(4)−Cu(2)−O(4)	156.1(2)
N(3)−Cu(1) N(1)	161.0(2)	N(5)−Cu(2)−O(7)	148.5(2)
N(2)−Cu(1) N(1)	81.6(2)	O(4)−Cu(2)−N(5)	91.8(2)
N(3)−Cu(1) O(1)	99.4(2)	O(4)−Cu(2)−N(4)	156.1(2)
N(2)−Cu(1)−O(1)	177.3(2)	N(5)−Cu(2)−N(4)	82.6(2)
N(1)−Cu(1)−O(1)	98.4(2)	O(4)−Cu(2)−O(7)	95.4(2)
O(1)−Cu(1)−O(3)	55.7(2)	N(5)−Cu(2)−O(7)	148.5(2)
O(1)−Cu(1)−N(2)	177.3(2)	N(4)−Cu(2)−O(7)	101.5(2)
N(1)−Cu(1)−N(3)	161.0(2)		

nitrates indicates that the ligand has become deprotonated at N(3), which shows the presence of just one proton. Each copper atom has four short equatorial bonds (<2 Å) and longer contacts to nitrate oxygens (Cu(1)−O(3) 2.489(4) Å; Cu(2)−O(9) 2.544(4) Å). The Cu(1)−N(3) distance (1.916(5) Å) is very short, as would be expected. The stereochemistry at both copper centers is best described as distorted square-pyramidal, despite the nominal tetrahedral distortion at Cu(2) (N(4)−Cu(2)−O(4) 156.1(2)°; N(5)−Cu(2)−O(7) 148.5(2)°).

The *trans* ligand arrangement is effectively locked into place by the coordination of the deprotonated anionic nitrogen N(3) to Cu(1). This leads to a large copper−copper separation (4.778(4) Å) and an almost flat structure, with a dihedral angle between the least-squares planes N(1)−C(5)−C(6)−N(2)−Cu(1) and N(4)−C(13)−C(12)−N(5)−Cu(2) of 165.2°.

Spectroscopy and Magnetism. All of the complexes exhibit rather complex infrared absorption patterns above 3100 cm^{-1} associated with both NH and OH vibrations. The ligands PAHAP (**1**) and PMHAP (**2**) each have two prominent NH absorptions at 3470 and 3268 (**1**) and 3465 and 3318 (**2**) cm^{-1}. A sharp doublet at 3566, 3500 cm^{-1} for **3** is associated with the lattice water molecule, while a broad, strong absorption envelope at 3346 cm^{-1} can be assigned to NH stretch. The NH vibrations can be clearly identified in the spectrum of **4**, which has no water, and appear as two pairs of peaks at 3353, 3309 cm^{-1} and 3231, 3189 cm^{-1}, suggesting the possibility of two different environments for the NH_2 groups in **4**. The bromide complex **5** clearly shows the presence of lattice water with a sharp doublet at 3579 and 3503 cm^{-1} and a rather complex absorption envelope in the range 3140−3340 cm^{-1} associated with NH absorptions. A strong, broad absorption with a prominent shoulder at 3490 cm^{-1} is associated with the

coordinated waters in **6**, while strong broad bands at 3338 and 3160 cm^{-1} are assigned to NH stretches. A sharp, single nitrate combination ($\nu_1 + \nu_4$) band[42] at 1763 cm^{-1} indicates that the nitrates are essentially ionic in nature in **6**. The azide complex **7** has a sharp single NH band at 3372 cm^{-1} and a broader absorption at 3100−3200 cm^{-1}, consistent with a single NH proton at a deprotonated nitrogen center and an NH_2 group. Azide bands at 2092 and 2031 cm^{-1} are consistent with terminally bound azides, probably in a local C_{2v} environment. A weak band at 1750 cm^{-1} indicates the presence of nitrate, but it is difficult to determine its role. The PMHAP nitrate complex **8** shows just one sharp NH absorption at 3376 cm^{-1}, associated with the hydrogen bonded to N(3), and no absorption associated with water. Three prominent nitrate combination bands are observed at 1770, 1757, and 1724 cm^{-1}, consistent with the presence of both monodentate and bidentate nitrates, although two bands are usually observed in each case.[42]

One characteristic infrared band for ligands containing 2-pyridyl fragments occurs at ≈990 cm^{-1}, associated with a pyridine ring breathing mode,[43] which becomes shifted to higher energies on coordination. This band occurring at 997 cm^{-1} for **1** and at 994 cm^{-1} for **2** is shifted to 1023 cm^{-1} for **3**, 1020 cm^{-1} for **4**, 1021 cm^{-1} for **5**, 1027 cm^{-1} for **6**, 1015 cm^{-1} for **7**, and 1010 cm^{-1} for **8**, indicating pyridine coordination in each case.

Solid state mull transmittance electronic spectra for **3**−**8** are quite similar, with one broad visible band in the range 690−730 nm, consistent with square or square-pyramidal coordination geometries. Aqueous solutions of **3**−**6** exhibit essentially identical spectra, with a broad absorption at 720 nm, consistent with the same solution species in each case and solvation of open coordination positions at each copper center. In DMF solution, however, the spectra are quite different (780 nm (**3**), 820 nm (**4**), 817 nm (**5**), 710 nm (**6**)), indicating incomplete solvation effects. The longer wavelength absorptions for **3**−**5** in DMF suggest the persistence of copper−halogen bonds in solution and for **4** a structure somewhat different from that of **3**. The most likely structure to resist solvation effects would be one with intramolecular halogen bridges, and a possible structure for **4** would involve two square-pyramidal copper centers in a pseudo-*cis* conformation with one or even two chlorine bridges. Molecular models suggest these are reasonable structural possibilities, which would create a relatively small angle between the two copper basal planes and not create any serious steric problems on the part of the two NH_2 groups. Despite the fact that reasonable crystals of **4** were obtained, none have so far permitted a structural determination. For **5**, the long-wavelength band (817 nm) suggests that the weak intramolecular bromine bridging structure may persist in solution.

The clear evidence for a deprotonated amino nitrogen in **7** suggests coordination of this center, and in keeping with the structure of **8**, a *trans* structural arrangement is predicted, with the ligand exhibiting tridentate behavior on one side and bidentate on the other (Figure 2a,c). The azide infrared bands suggest two terminal azides bound to one copper center, and it is reasonable to assume that the nitrate is bound, probably in a monodentate fashion, at the other copper center in a structural arrangement similar to **8**. It is of interest to note that an aqueous solution of **8** has a pH of 5.5 and a visible absorption at 683 nm. However, acidifying the solution slightly (pH = 4.5) shifts the visible band to 724 nm, consistent with the neutral species **3**−**6**, but also in exactly the same position as that associated with the neutral complex $[Cu_2(PMHAP)(H_2O)_4](NO_3)_4$.[44]

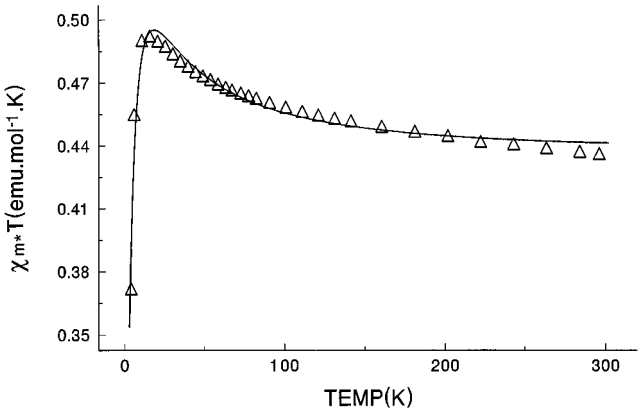

Figure 9. Variable-temperature magnetic data for **3**. The solid line was calculated from eq 1 with $g = 2.138(5)$, $2J = 24.4(16)$ cm^{-1}, TIP = 20×10^{-6} emu, $\Theta = -1.85$ K, and $10^2R = 1.3$ ($R = [\sum(\chi_{obs} - \chi_{calc})^2/\sum\chi_{obs}^2]^{1/2}$).

The room temperature magnetic moments for **3**−**6** are close to the normal value for an uncoupled copper(II) system (1.87 μ_B (**3**), 1.77 μ_B (**4**), 1.87 μ_B (**5**), 1.85 μ_B (**6**)) and might suggest the absence of spin exchange. **7** and **8** have much lower room-temperature magnetic moments (1.42 and 1.57 μ_B, respectively) indicative of net antiferromagnetic coupling. A plot of $\chi_m T$ versus temperature for **3** is illustrated in Figure 9, and the rise in $\chi_m T$ values from 0.44 emu·mol^{-1}·K at 296 K to 0.492 emu·mol^{-1}·K at 16 K clearly indicates the presence of intramolecular ferromagnetic coupling. The drop at lower temperatures suggests the presence also of weak antiferromagnetism, which only appears in this temperature range. Fitting of the data to a modified Bleaney−Bowers equation (eq 1)[45] was carried out

$$\chi_m = \frac{N\beta^2 g^2}{3k(T-\Theta)}[1 + {}^1/_3 \exp(-2J/kT)]^{-1}(1-\rho) + \frac{[N\beta^2 g^2]\rho}{4kT} + N\alpha \quad (1)$$

and the intramolecular ferromagnetic coupling confirmed with $2J = 24.4(2)$ cm^{-1} ($g = 2.138(5)$, $2J = 24.4(2)$ cm^{-1}, TIP = 20×10^{-6}emu, $\Theta = -1.85$ K, $10^2R = 1.3$; R = $[\sum(\chi_{obs} - \chi_{calc})^2/\sum\chi_{obs}^2]^{1/2}$). The solid line in Figure 9 was calculated using these parameters. The ferromagnetic interaction is associated with intradinuclear exchange via the N−N bridge and not the weak orthogonal interaction between each dinuclear unit. In fact, the small Curie−Weiss-like correction term Θ is negative, consistent with the presence of a very small intermolecular antiferromagnetic component. This can be assigned to the weak interdimer bridging connection via Cl(1), which is the only significant intermolecular contact. A similar bridging arrangement, with long axial copper−bromine contacts (Cu−Br 3.033 Å), in the complex $[Cu(4\text{-Metz})_2Br_2]_2$[46] also leads to weak antiferromagnetic coupling ($-2J = 2.4$ cm^{-1}).

Variable-temperature magnetism of $[Cu_2(PAHAP)Br_4]\cdot H_2O$ (**5**) is very similar to that of **3**, with χT rising steadily from a value of 0.43 emu·mol^{-1}·K at 295 K to 0.62 emu·mol^{-1}·K at 3.9 K, indicative again of intramolecular ferromagnetic coupling. The data were fitted to eq 1 to give $g = 2.067(5)$, $2J = 22(2)$

(42) Lever, A. B. P.; Mantovani, E.; Ramaswamy, B. S. *Can. J. Chem.* **1971**, *49*, 1957.
(43) Katritzky, A. R.; Hands, A. R. *J. Chem. Soc.* **1958**, 2202.
(44) Xu, Z.; Thompson, L. K. Unpublished results.
(45) Bleaney, B.; Bowers, K. D. *Proc. R. Soc. London, Ser. A* **1952**, *214*, 451.
(46) Marsh, W. E.; Bowman, T. L.; Harris, C. S.; Hatfield, W. E.; Hodgson, D. J. *Inorg. Chem.* **1981**, *20*, 3864.

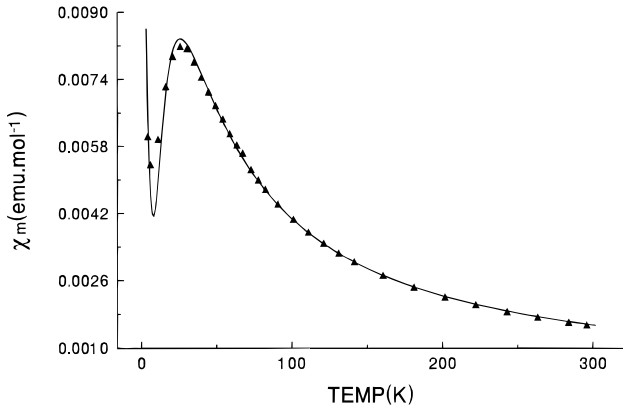

Figure 10. Variable-temperature magnetic data for **6**. The solid line was calculated from eq 1 with $g = 2.25(1)$, $-2J = 27.4(6)$ cm^{-1}, $\rho = 0.054$, TIP $= 36 \times 10^{-6}$ emu, $\Theta = -6.5$ K, and $10^2R = 1.0$.

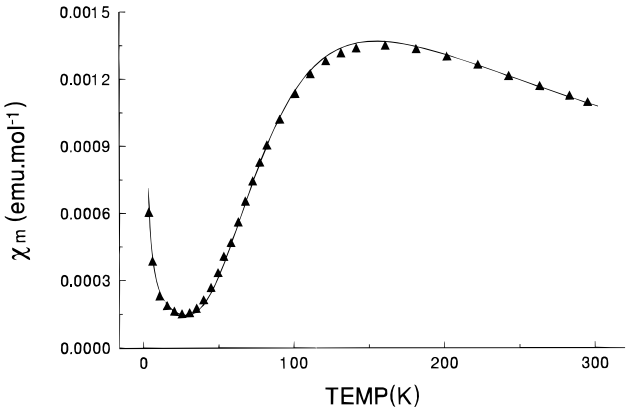

Figure 11. Variable-temperature magnetic data for **8**. The solid line was calculated from eq 1 with $g = 2.07(4)$, $-2J = 173(3)$ cm^{-1}, $\rho = 0.0048$, TIP $= 68 \times 10^{-6}$ emu, $\Theta = -0.76$ K, and $10^2R = 0.85$.

cm^{-1}, $\rho = 0.000\,03$, TIP $= 45 \times 10^{-6}$ emu, $\Theta = 0.56$ K, and $10^2R = 0.9$. No apparent significant intermolecular contacts appear in the structure of **5**, and this is mirrored in the magnetic data.

The variable-temperature magnetic properties of **6** are in sharp contrast to those of **3**. A plot of χ_m versus temperature is illustrated in Figure 10 and reveals a maximum in susceptibility at ≈25 K. This is clearly indicative of dominant antiferromagnetic exchange. The data were fitted successfully to eq 1 with $g = 2.25(1)$, $-2J = 27.4(6)$ cm^{-1}, $\rho = 0.054$, TIP $= 36 \times 10^{-6}$ emu, $\Theta = -6.5$ K, and $10^2R = 1.0$. The solid line in Figure 10 was calculated with these parameters. The necessity for the inclusion of a significant Θ correction in the fitting procedure raises the question of the appropriateness of the magnetic model, but it is clear from the structure that the Bleaney−Bowers equation should realistically interpret the exchange situation. Therefore the negative Θ value indicates an intermolecular antiferromagnetic interaction. Although there are many intermolecular hydrogen-bonding interactions (vide infra), a logical pathway for antiferromagnetic coupling would involve a direct connection between the copper magnetic orbitals. Only one such connection occurs between N(3) and Cu(1) (via O(2)−O(6)−N(5)−O(8)). This is clearly very long (six bonds and two hydrogen bonds) but is not unreasonable given the weak nature of the interaction.

The magnetic properties of **4** are also surprisingly quite different from those of **3**, even though the only analytical difference between the two compounds is the clearly defined absence of water in **4**. Variable-temperature magnetism of **4** shows a maximum in the χ versus temperature profile at ≈45 K, indicative of antiferromagnetic coupling, but stronger than in **6**. A reasonable fit of the data to eq 1 was achieved, and the best fit gave $g = 2.101(6)$, $-2J = 44.0(3)$ cm^{-1}, $\rho = 0.00005$, TIP $= 60 \times 10^{-6}$ emu, and $\Theta = -7.5$ K ($10^2R = 1.3$). The stronger antiferromagnetism in **4**, comparable with that observed for $[Cu_2(PMK)Cl_4]$,[21] suggests a structure different from that of **3**, with a different angle between the magnetic planes or an additional magnetic bridge. The suggested chlorine-bridged structure for **4** would be consistent with this situation, if the bridge connected the two magnetic orbitals directly. The significant Θ value, larger than that for **3**, indicates a stronger intermolecular exchange component, suggesting possible interdimer associations as well. We await a structural determination of this compound.

The azide complex $[Cu_2(PAHAP\text{-}H)(N_3)_2{\cdot}NO_3]$ (**7**) has a pronounced maximum in susceptibility at ≈180 K, clearly indicating antiferromagnetic exchange. A good fit to eq 1 gave $g = 2.035(3)$, $-2J = 207.4(7)$ cm^{-1}, $\rho = 0.0013$, TIP $= 78 \times 10^{-6}$ emu, and $\Theta = -0.4$ K ($10^2R = 0.7$). The strong antiferromagnetic coupling is consistent with the proposed *trans* conformation for this compound (vide infra).

The plot of molar susceptibility versus temperature for **8** is illustrated in Figure 11. The maximum at ≈160 K is indicative of fairly strong intramolecular antiferromagnetic coupling, and the solid line corresponds to a good data fit to eq 1 for $g = 2.07(4)$, $-2J = 173(3)$ cm^{-1}, $\rho = 0.0048$, TIP $= 68 \times 10^{-6}$ emu, and $\Theta = -0.76$ K ($10^2R = 0.85$). The strong antiferromagnetic coupling is consistent with the *trans* structure of this compound, in which there is clearly good overlap of the magnetic copper orbitals and the p orbitals of the diazine bridge (vide supra).

The radically different magnetic behavior of **3** and **5** compared with that of **6** and **8**, and also with that of the complex $[Cu_2(PMK)Cl_4]$ (**9**),[21] prompted us to search the literature for related examples of dinuclear systems with a single N−N group as the only bridge between the copper(II) centers. Although a handful of compounds have been structurally characterized, variable-temperature magnetic studies, and related structural studies, have previously been limited to $[Cu_2(PMK)Cl_4]$ (**9**)[21] and $[Cu_2(HL')Cl_3(H_2O)]{\cdot}1.5H_2O$ (**10**)[25] (H_2L' = bis(methyl 2-pyridyl ketone) carbonohydrazone). Both of these compounds are antiferromagnetically coupled ($-2J = 52(4)$ and 213.3 cm^{-1}, respectively), but to a dramatically different extent. This is clearly related to the angle between the magnetic planes in these two complexes. For **9**, the Cu−N−N−Cu torsion angle is 70.8°, indicating an acute angle between the magnetic planes. In contrast, the magnetic orbitals in **10** are almost coplanar. In both cases, the magnetic ground state for the copper centers is of the $d_{x^2-y^2}$ type. **3**, **5**, **6**, and **8** are consistent with this situation, in that the twist angles between the copper coordination planes are 77.1, 75.0, 100.2, and 165.2°, respectively, despite the fact that the terminal ligands are different.

To test the hypothesis that the twist angle between the magnetic planes is the major factor in determining the type and extent of coupling, molecular orbital calculations have been carried out at the extended Hückel[47] level for **3**, **5**, **6**, and **8**, and also for the complex $[Cu_2(PMK)Cl_4]$, using the *exact* crystallographic coordinates. The data set for **6** was simplified by the removal of the axial water molecules (O(9)), which did not alter the copper magnetic ground state or the molecular geometry. The two highest antibonding triplet state molecular orbitals for **3**, which are responsible for the magnetic properties, are dominated by p orbital components on the diazine nitrogens and the pyridine nitrogens. The molecular twist along the N−N

(47) Mealli, C.; Proserpio, D. M. *J. Chem. Educ.* **1990**, *67*, 399.

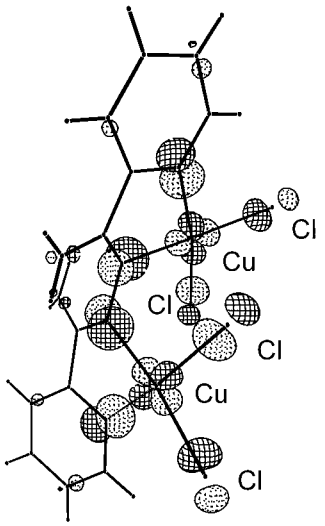

Figure 12. The symmetric SOMO for **3** ($E = -11.422$ eV).

bond results in misalignment of the adjacent p orbitals in the N−N bond, almost amounting to a situation of orthogonality. With very limited overlap between these orbitals, it is no surprise that the energy difference between the symmetric and antisymmetric MO's is very small ($\Delta E = 29$ meV). The symmetric molecular orbital combination is illustrated in Figure 12. A similar situation exists for **5**, again with a small energy difference between the triplet state SOMO's (46 meV). The two comparable highest energy molecular orbitals for **6** are again dominated by p orbital components on the pyridine ring and diazine nitrogens, but because of the flatter nature of the molecule, overlap between the diazine p orbitals is enhanced such that the difference in energy between the symmetric and antisymmetric magnetic MO's is substantially larger ($\Delta E = 153$ meV). A similar calculation for $[Cu_2(PMK)Cl_4]$ (**9**) indicates a large energy difference between the symmetric and antisymmetric molecular orbitals ($\Delta E = 269$ meV), consistent with the stronger antiferromagnetic coupling. However a direct comparison of ΔE values here is inappropriate because of the different ligands. The molecular orbital picture for **8** is complicated by the presence of a different diazine ligand and the additional copper−nitrogen bond (Cu(1)−N(3); 1.916(5) Å), which is very short, and the antisymmetric MO shows a significant contribution from p orbitals in the framework Cu(1)−N(3)−C(13)−N(4)−Cu(2). This, combined with the almost flat nature of the molecule, leads to a very large difference in energy between the two magnetic molecular orbitals (453 meV), consistent with the strong antiferromagnetic coupling observed for this complex. However, the strong exchange in this case appears not to be due entirely to the diazine bridge.

The validity of these observations, within a limited data set, is best examined in the context of a set of molecular models and appropriate molecular orbital calculations. A simple chloro-model system that combines the essential features of the ligand (i.e., the two sp^2 nitrogen centers linked by a single N−N bond) and the copper square planes is illustrated in Figure 13. Averaged bond distances from existing and related structures have been used (e.g., Cu−N 2.00 Å, Cu−Cl 2.25 Å, N−N 1.43 Å, and C═N 1.30 Å), and the only molecular geometrical change involves rotation of each copper plane, in conjunction with the CH_2 group, as a fixed unit, around the N−N bond. The energies of the appropriate SOMO's in the triplet state (Φ_s and Φ_{as}) are plotted as a function of the fold angle (τ; dihedral angle between the copper planes) in Figure 13. Similar calculations for analogous bromo and aquo models (cf. **5** and **6**, respectively), with appropriate bond lengths, were also carried

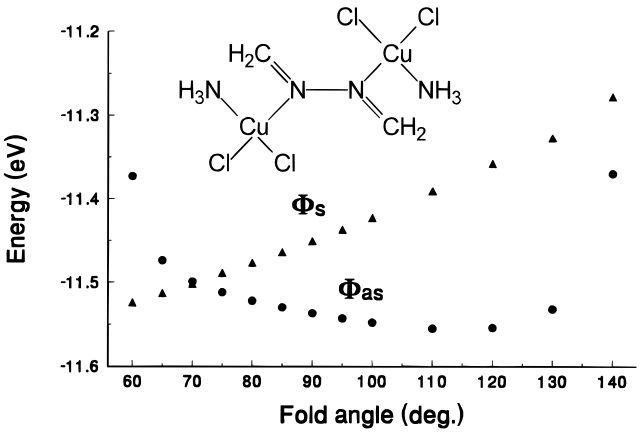

Figure 13. Plot of orbital energies (Φ_s, Φ_{as}) against fold angle for the chloride model.

out. In each case, for comparable τ values the SOMO's bear a striking resemblance to those associated with **3**, **5**, and **6**.

The crossover of the symmetric and antisymmetric molecular orbital energies occurs at 70° for the chloro model (Figure 13). This is the point at which the J_{AF} term is effectively zero. A smooth variation in orbital energies occurs between about 65 and 120°, but outside these limits the antisymmetric molecular orbital energy increases rapidly, consistent with steric interactions between the chlorine and CH_2 groups approaching the *trans* conformation and intramolecular chlorine bridging interactions approaching the *cis* conformation. A similar energy profile occurs for the bromo model, with an energy crossover at 70° also, indicating no significant effect on changing the halogen. The model aquo complex is also very similar, with a smooth variation in symmetric and antisymmetric molecular orbital energies in the fold angle range 40−140°, due mainly to the reduced steric constraints approaching the *cis* and *trans* conformation limits, and an energy crossover at 65°.

These calculations may be used in conjunction with the orbital model for the exchange interaction (eq 2) between two copper-

$$J = J_F + J_{AF} = -2K_{12} + (\epsilon_s - \epsilon_a)^2/(J_{11} - J_{12}) \qquad (2)$$

(II) centers,[48−50] in which the exchange integral J can be correlated with geometric distortions. J can be written as the sum of two terms: J_F, being the term defined by the exchange integral between the two localized molecular orbitals, which is always ferromagnetic, and J_{AF}, which comprises two components, the square of the difference in energy between the two molecular orbitals (ϵ_s, ϵ_a) in the triplet state and the difference in Coulomb integrals between the localized molecular orbitals (J_{11}, J_{12}). In correlations within a series of related compounds, the term that changes most is $(\epsilon_s - \epsilon_a)^2$ and the other terms are considered to be largely invariant. The energy difference between the two molecular orbitals calculated above is therefore a major function of the J_{AF} term.

A comparison of the exchange situation for **3**, **5**, and **6** with the model studies provides a satisfying rationale for the dramatically different magnetic properties of these compounds. The positions of the coordination planes are fixed with respect to the two nitrogen donors, as a result of the formation of the two five-membered chelate rings. The net effect is that the copper magnetic planes simply rotate about the N−N bond. This is modeled by fixing the relative positions of the NH_3 and the

(48) Hay, P. J.; Thibeault, J. C.; Hoffmann, R. *J. Am. Chem. Soc.* **1975**, *97*, 4884.
(49) Kahn, O.; Briat, B. *J. Chem. Soc., Faraday Trans.* **1976**, *72*, 268.
(50) Kahn, O.; Briat, B. *J. Chem. Soc., Faraday Trans.* **1976**, *72*, 1441.

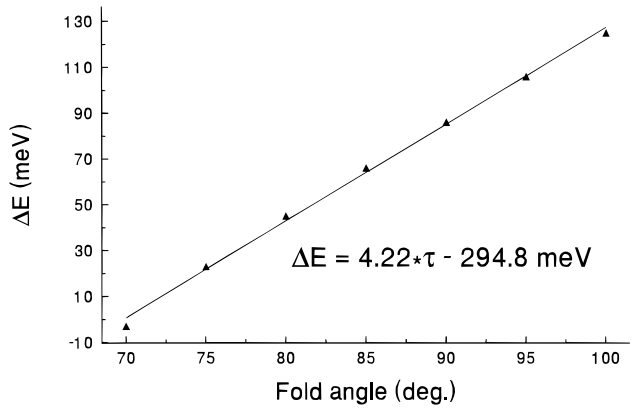

Figure 14. Plot of energy difference ($\Phi_s - \Phi_{as}$) for the chloride model.

N═CH_2 groups as the metal plane rotates (Figure 13). For **3**, the fold or twist angle, based on the five-membered chelate ring, is 77.1° ($E_{as} < E_s$; $\Delta E = 29$ meV), with the antisymmetric molecular orbital lower in energy. A plot of $E_s - E_{as}$ versus fold angle for the chloro-model complex is illustrated in Figure 14 and shows a good straight-line relationship in the range 70−100° ($\Delta E = 4.22\tau - 294.8$ meV). For a fold angle (τ) of 77.1°, the value of ΔE calculated from this line is 30.6 meV, in very close agreement with the value calculated for **3**. This small difference in energy, in the same relative position in the energy profile (i.e., $E_{as} < E_s$), clearly indicates that the J_{AF} term for **3** is very small, giving a very reasonable explanation as to why this compound is ferromagnetic. An exactly analogous situation exists for **5** ($\tau = 75.0°$), with a calculated ΔE value of 29 meV from the model system ($\Delta E = 3.01\tau - 198.0$ meV), compared with 46 meV based on the structure itself.

For **6**, the situation is quite different. The calculated energy difference between the symmetric and antisymmetric triplet state molecular orbitals is 153 meV for a fold angle of 100.2°, while for a comparable model system (Figure 13 with Cl replaced by H_2O), a linear regression of $E_s - E_{as}$ as a function of fold angle in the range 65−120° ($\Delta E = 4.11\tau - 275.6$ meV) gives a ΔE value of 137 meV (100.2°), in close agreement. This relatively large energy difference for **6** leads to a large value for J_{AF}, which clearly dominates the overall exchange situation, leading to net antiferromagnetic coupling. It is very significant that the tetranuclear complex $\{[Cu(L\text{-}H)]_4(NO_3)_4(H_2O)_8\}$[30] has an effective fold angle between the copper square planes of ≈90°, between those of **3** and **6**, and exhibits no coupling. Clearly, J_{AF} and J_F for this system are approximately the same.

Optimal alignment of the nitrogen p orbitals, and the metal magnetic orbitals, might reasonably be expected at large fold angles approaching molecular planarity. **8** is almost flat and exhibits much stronger antiferromagnetic coupling than observed for **3**, **5**, and **6**. This is also consistent with the large energy difference between the triplet state molecular orbitals (453 meV) calculated for this complex. However, the possibility of a longer, four-bond secondary exchange route (Cu(1)−N(3)−C(13)−N(4)−Cu(2)) must also be considered in this case. Complex **10** has a comparable exchange integral ($-2J = 213.3$ cm^{-1})[25] and a similar additional four-bond potential exchange route.

The exchange process must be dominated by σ interactions, because of the hybridization situation that exists at the diazine nitrogens, and so the extent of exchange will, of necessity, be dependent upon the extent of overlap of the appropriate diazine nitrogen p orbitals. The free-ligand HOMO is a σ-bonding molecular orbital with an energy comparable to that of the metal d orbitals and involves diazine nitrogen p orbital components which point along the C═N bonds. Interaction of the copper $d_{x^2-y^2}$ type orbitals with these two p orbitals leads to the formation of the antisymmetric and symmetric triplet state molecular orbitals (Φ_s; Figure 12), in which the p orbitals align themselves according to the relative orientation of the copper d orbital planes. The extent of overlap between the p orbitals along the single N−N bond is therefore dependent upon the fold angle between the magnetic copper planes, and so, at some angle, effective p orbital orthogonality is achieved.

For the model complexes, these angles fall in a narrow range (65−75°), less than 90°, which is reasonable on the basis of the trigonal nitrogen atom geometry. **3** and **5** have fold angles (77.1 and 75.0°, respectively) very close to this situation, whereas for complexes **6** and **8** the much larger twist leads to more effective p orbital overlap.

Conclusion

A spin exchange situation in a dicopper(II) system bridged only by a single N−N bond, in which the exchange mechanism is dominated by σ interactions, was investigated as a function of twist of the copper magnetic planes about this bond. At an acute angle approaching orthogonality between the nitrogen p orbitals, ferromagnetic coupling was observed, while at much larger angles significant overlap between the nitrogen p orbitals was seen to lead to net antiferromagnetic coupling. Molecular orbital calculations on comparable models successfully reproduced this magnetic situation and indicated that, with appropriately chosen coligands, which can systematically influence the molecular twist, the specific synthesis of ferromagnetic dinuclear complexes involving simple N−N bridging ligands is possible.

Acknowledgment. We thank the Natural Sciences and Engineering Research Council of Canada for financial support of this study and Dr. Glenn P. A. Yap at the University of Windsor for structural data on complex **8**.

Supporting Information Available: Tables listing detailed crystallographic data, atomic positional parameters, anisotropic thermal parameters, and bond lengths and angles (22 pages). Ordering information is given on any current masthead page.

IC970235K